


 Cite this: *RSC Adv.*, 2022, **12**, 24590

Carotane sesquiterpenoids A–G from the desert endophytic fungus *Fusarium* sp. HM 166†

 Bing-Wen Zhang,^a Li Jiang,^a Zhuang Li,^a Xue-Hui Gao,^a Fei Cao,^a Xin-hua Lu,^c Wen-Bin Shen,^c Xue-Xia Zhang,^c Fan-Dong Kong^{*b} and Du-Qiang Luo^{ib} ^{*a}

Seven undescribed carotane sesquiterpenoids named fusanoids A–G (1–7), along with one known analog (8) and two known sesterterpenes (9 and 10), were isolated from the fermentation broth of the desert endophytic fungi *Fusarium* sp. HM166. The structures of the compounds, including their absolute configurations, were determined by spectroscopic data, single-crystal X-ray diffraction analysis, and ECD calculations. Compound 10 showed cytotoxic activities against human hepatoma carcinoma cell line (Huh-7) and human breast cell lines (MCF-7 and MDA-MB-231), and compound 2 showed cytotoxic activity against MCF-7, while compounds 4–9 were inactive against all the tested cell lines. Compounds 4 and 10 showed potent inhibitory activities against the IDH1^{R132H} mutant.

 Received 1st May 2022
 Accepted 9th August 2022

DOI: 10.1039/d2ra02762c

rsc.li/rsc-advances

Introduction

It is still very popular to use the synthetic structure of natural products or natural products to discover or develop solid drugs.^{1,2} A large number of natural product drugs synthetic variations are actually produced by microbial and/or microbial interactions with the host, so the scope of research in the field of natural products should be expanded.³ Endophytic fungi are the fungi that live in different tissues or organs of host plants. They also include saprophytic fungi that live on the surface at a certain stage of their life cycle, as well as latent proto fungi and mycorrhizal fungi that do not harm the host temporarily.^{4,5}

Studies have shown that endophytic fungi may play a potential role in tolerance to plant host stress.⁶ Deserts are characterized by very limited availability of water and nutrients, extreme temperatures, long periods of sunshine, and strong winds and high ultraviolet (UV) radiation. Desert habitats

represent one of the most challenging environments for the growth of plants.^{6–8} Desert plants adapt to harsh environmental conditions and play an important role in ecosystems. Compared with plant endophytic fungi in common areas, desert microorganisms have different species, functions, and strong resistance to stress, and can grow in water shortage environments. In recent years, a large number of novel secondary metabolites, such as polyketides, alkaloids, terpenes, have been discovered from desert plant endophytic fungus. These metabolites have a variety of potent biological activities and ecological effects, such as cytotoxic, antivirus, and antifungal.^{9–13}

In the search for undescribed bioactive natural products from desert endophytic fungi, we studied *Fusarium* sp. HM166, which was isolated from the small quinoa in the Inner Mongolia Autonomous Region of Western China. As a result, eight terpenoids, including seven undescribed sesquiterpenes (1–7),

^aCollege of Life Science, Key Laboratory of Microbial Diversity Research and Application of Hebei Province, Hebei University, Baoding 071002, People's Republic of China. E-mail: duqiangluo@163.com

^bKey Laboratory of Chemistry and Engineering of Forest Products, State Ethnic Affairs Commission, Guangxi Key Laboratory of Chemistry and Engineering of Forest Products, Guangxi Collaborative Innovation Center for Chemistry and Engineering of Forest Products, School of Chemistry and Chemical Engineering, Guangxi Minzu University, Nanning 530006, Republic of China. E-mail: kongfandong0127@126.com

^cNew Drug Research & Development Center of North China Pharmaceutical Group Corporation, National Microbial Medicine Engineering & Research Center, Hebei Industry Microbial Metabolic Engineering & Technology Research Center, Key Laboratory for New Drug Screening Technology of Shijiazhuang City, Shijiazhuang 052165, Hebei, China. E-mail: luxinhua89@yeah.net

† Electronic supplementary information (ESI) available: UV, IR, HRESIMS, NMR spectra of compounds 1–7; ECD calculations of compounds 1–7. CCDC 2080924. For ESI and crystallographic data in CIF or other electronic format see <https://doi.org/10.1039/d2ra02762c>

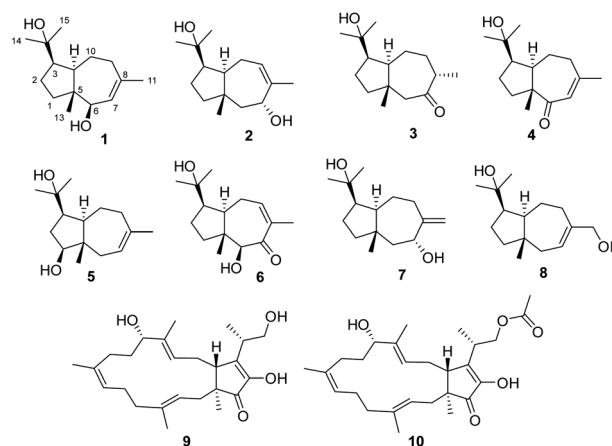


Fig. 1 Structures of compounds 1–10.



and three known compounds, (+)-schisanwilsonene A (**8**),¹⁴ (–)-terpestacin (**9**), and fusaproliferin (**10**),¹⁵ were isolated and identified (Fig. 1). Herein, the isolation, structural elucidation, and bioactivity of these compounds were reported.

Results and discussion

Compound **1** was obtained as colorless needles, had the molecular formula C₁₅H₂₆O₂, as established by its positive HRESIMS spectrum at *m/z* 261.1825 (calcd for C₁₅H₂₆O₂Na), indicating three degrees of unsaturation. The infrared (IR)

spectrum showed the presence of hydroxy (3362 cm⁻¹) and olefin (2964 cm⁻¹) groups. The ¹H NMR and ¹³C NMR spectra (Tables 1 and 2), in association with the HSQC spectrum, indicated 15 carbon signals, including four methyls ($\delta_{C/H}$ 27.1/1.74, Me-11; 14.4/0.80, Me-13; 32.3/1.14, Me-14; 26.8/1.17, Me-15), four methylenes (δ_C 39.5, C-1; 27.8, C-2; 36.9, C-9; 24.1, C-10), four methines (δ_C 54.2, C-3; 55.2, C-4; 81.7, C-6; 131.7, C-7), and three quaternary carbons (δ_C 48.8, C-5; 136.6, C-8; 75.0, C-12). The ¹H NMR signal at δ_H 5.25 and ¹³C NMR signals at δ_C 131.7 and 136.6 suggested a trisubstituted double

Table 1 The ¹H NMR data for 1–7

	1 ^a	2 ^a	3 ^b	4 ^a	5 ^a	6 ^a	7 ^a
	δ_H (J in Hz)	δ_H (J in Hz)	δ_H (J in Hz)	δ_H (J in Hz)	δ_H (J in Hz)	δ_H (J in Hz)	δ_H (J in Hz)
1a	1.31, overlap	1.31, m	1.43, overlap	1.72, overlap	3.51, dd (6.6, 11.2)	1.58, m	1.30, overlap
1b	1.66, m	1.47, m	1.48, overlap	1.74, overlap		1.79, m	1.44, overlap
2a	1.33, overlap	1.43, m	1.57, overlap	1.40, m	1.39, m	1.47, m	1.69, m
2b	1.74, overlap	1.68, m	1.79, overlap	1.77, m	1.93, m	1.75, m	1.48, m
3	2.43, m	2.34, m	2.42, overlap	2.34, m	2.25, overlap	2.46, m	2.30, m
4	1.82, m	1.85, ddd (12.3, 12.3, 2.7)	1.98, m	2.41, m	1.87, dd (11.6, 12.5)	2.47, m	1.88, ddd (3.9, 12.5, 13.4)
6a	3.86, br s	1.38, dd (11.7, 11.7)	2.54, d (14.5)		1.67, br d (13.8)	3.88, s	1.23, dd (10.3, 13.1)
6b		1.96, dd (4.1, 11.7)	2.48, d (14.5)		2.21, overlap		2.11, dd (6.4, 13.1)
7	5.25, br s	4.28, br d (11.7)		5.81, s	5.40, m		4.17, dd (6.4, 10.3)
8			2.48, overlap				
9a	1.89, m	5.54, d (8.1)	1.44, overlap	2.28, m	2.09, m	6.50, br d (7.4)	2.23, m
9b	2.06, m		1.93, m	2.41, m	1.96, m		2.29, m
10a	1.42, m	2.15, m	1.72, m	2.02, m	2.26, m	3.17, m	1.57, m
10b	2.33, m	2.81, ddd (2.7, 8.6, 16.8)	2.57, m	2.56, m	1.53, m	2.50, m	2.39, m
11a	1.74, s	1.76, s	1.08, d (7.2)	1.89, s	1.73, s	1.88, s	4.88, br s
11b							5.04, br s
13	0.80, s	0.93, s	0.97, s	1.16, s	0.72, s	0.77, s	0.91, s
14	1.14, s	1.16, s	1.19, s	1.25, s	1.14, s	1.23, s	1.16, s
15	1.17, s	1.18, s	1.22, s	1.27, s	1.18, s	1.24, s	1.19, s

^a ¹H (600 MHz) NMR data in CD₃OD. ^b ¹H (600 MHz) NMR data in CDCl₃.

Table 2 The ¹³C NMR data for 1–7

	1 ^a	2 ^a	3 ^b	4 ^a	5 ^a	6 ^a	7 ^a
Position	δ_C	δ_C	δ_C	δ_C	δ_C	δ_C	δ_C
1	39.4, CH ₂	43.3, CH ₂	43.1, CH ₂	35.8, CH ₂	79.9, CH	39.6, CH ₂	43.8, CH ₂
2	27.8, CH ₂	28.0, CH ₂	28.4, CH ₂	27.0, CH ₂	35.8, CH ₂	28.0, CH ₂	28.2, CH ₂
3	54.2, CH	53.9, CH	53.5, CH	52.1, CH	49.0, CH	54.0, CH	54.0, CH
4	55.2, CH	51.5, CH	56.1, CH	44.3, CH	55.8, CH	49.1, CH	53.1, CH
5	48.8, C	43.4, C	42.3, C	56.3, C	45.4, C	47.5, C	43.9, C
6	81.5, CH	52.5, CH ₂	58.1, CH ₂	208.0, C	40.8, CH ₂	87.3, CH	51.5, CH ₂
7	131.7, CH	70.6, CH	218.6, C	127.1, C	123.5, CH	204.3, C	74.1, CH
8	136.6, C	141.4, C	48.4, CH	152.2, C	140.6, C	134.9, C	155.0, C
9	36.9, CH ₂	126.3, CH	27.1, CH ₂	35.5, CH ₂	37.0, CH ₂	143.4, CH	34.0, CH ₂
10	24.1, CH ₂	27.8, CH ₂	18.9, CH ₃	22.8, CH ₂	24.3, CH ₂	29.9, CH ₂	27.7, CH ₂
11	27.1, CH ₃	23.5, CH ₃	74.1, C	28.3, CH ₃	27.4, CH ₃	21.9, CH ₃	113.1, CH ₂
12	75.0, C	74.8, C	21.2, CH ₃	73.9, C	74.8, C	74.3, C	74.6, C
13	14.4, CH ₃	18.9, CH ₃	11.1, CH ₃	20.1, CH ₃	13.5, CH ₃	14.0, CH ₃	19.7, CH ₃
14	32.3, CH ₃	32.4, CH ₃	32.1, CH ₃	32.5, CH ₃	32.1, CH ₃	32.9, CH ₃	32.0, CH ₃
15	26.8, CH ₃	27.2, CH ₃	27.3, CH ₃	27.2, CH ₃	27.1, CH ₃	27.1, CH ₃	27.7, CH ₃

^a ¹³C (150 MHz) NMR data in CD₃OD. ^b ¹³C (150 MHz) NMR data in CDCl₃.



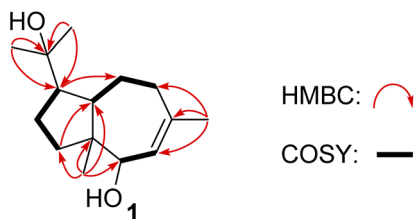


Fig. 2 Key ^1H - ^1H and HMBC correlations of **1**.

bond. The other two degrees of unsaturation were due to the presence of two rings in the structure. The presence of 5/7 bicyclic ring system was determined by COSY correlations (Fig. 2) of H_2 -1/ H_2 -2/ H -3/ H -4/ H_2 -10/ H_2 -9 and H -7/ H -6 as well as HMBC correlation from H_3 -13 to C-1, C-4, C-5, and C-6 and H_3 -11 to C-7, C-8, and C-9, which also assigned the locations of CH_3 -13 and CH_3 -11 at C-5 and C-8, respectively. The presence of a hydroxyl at C-6 was deduced by the chemical shifts of CH -6 ($\delta_{\text{C}/\text{H}}$ 81.7/3.86). The presence of a 2-hydroxypropan-2-yl group at C-3 was suggested by the HMBC correlations from both H_3 -14 and H_3 -15 to C-3 and C-12. ROESY correlations (Fig. 3) of H_3 -14 with H_2 -10 and H -6 with H -4 and H -1 suggested the same orientations of H -3, H -4, and H -6 as well as the opposite orientations of H_3 -13 to H -4. This was confirmed by ECD spectrum calculation by the TDDFT methodology at the CAM-B3LYP/6-311++G(2d,P) level in MeOH, the result of which showed good agreement with the experimental one (Fig. 5). Finally, this inference was further confirmed by the X-ray diffraction experiment using the anomalous scattering of $\text{Cu K}\alpha$ radiation, which also indicating the (3*R*,4*R*,5*R*,6*R*)-**1** absolute configuration (Fig. 4).

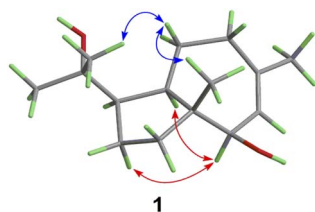


Fig. 3 Key ROESY correlations of **1**.

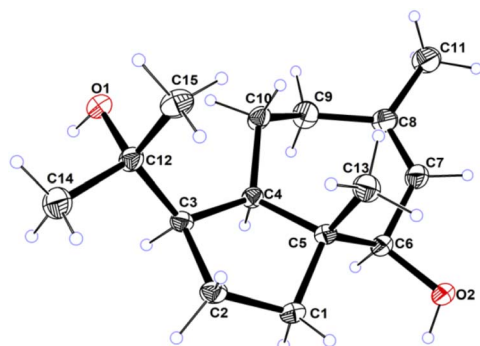


Fig. 4 ORTEP drawing of compound **1**.

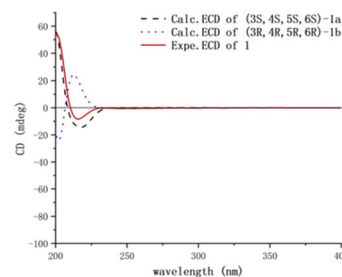


Fig. 5 Calculated and experimental ECD spectra of **1**.

Compound **2** was obtained as a colorless oil. The molecular formula of **2** was established to be the same as that of **1** according to its positive HRESIMS spectrum, with three degrees of unsaturation. The ^1H and ^{13}C NMR data (Tables 1 and 2) were also quite similar to those of **1**, indicating that they shared the same carbon skeleton. Detailed analysis of the 2D NMR data (Tables 1 and 2) of **2** revealed HMBC correlations from H_3 -13 to C-1, C-4, C-5, and the sp^3 methylene carbon C-6 as well as COSY correlations of H_2 -6 with the hydroxylated methine C-7 ($\delta_{\text{C}/\text{H}}$ 70.6/4.28) and H_2 -10 with the olefinic methine proton H -9 ($\delta_{\text{C}/\text{H}}$ 126.3/5.54). These data suggested the presence of C-8/C-9 double bond and C-7 hydroxyl, which were different from those of compound **1**. Consequently, the planar structure of **2** was established as shown in Fig. 1. ROESY correlations (Fig. S10[†]) of H_3 -14/ H -10a, H_3 -13/ H -10a, and H_3 -13/ H -7 led to the assignment of the relative configuration of **2**. The absolute configuration for **2** was also proposed by a comparison of the experimental ECD spectrum with the calculated ECD spectra (Fig. S11[†]) for **2** and *ent*-**2**. The experimental ECD spectrum of **2** was nearly identical to the calculated ECD one for **2**, clearly indicating the (3*S*,4*R*,5*S*,6*R*)-absolute configuration.

Compound **3** was obtained as a yellow oil, had the molecular formula $\text{C}_{15}\text{H}_{26}\text{O}_2$ on the basis of HRESIMS, same as that of **2**. The ^{13}C NMR data of **3** were also similar to those of **2**, suggesting that they bear similar structure. However, in the NMR spectra of **3**, the signals for the C-7 hydroxyl methine and the C-8/C-9 double bond of **2** were missing. Instead, a ketone carbonyl (δ_{C} 218.5), a sp^3 methine ($\delta_{\text{C}/\text{H}}$ 48.4/2.48), and a sp^3 methylene ($\delta_{\text{C}/\text{H}}$ 27.1/1.44, 1.93) were observed, suggesting the replacement of the C-7 hydroxyl methine and C-8/C-9 double bond of **2** by C-7 ketone carbonyl and CH -8/ CH_2 -9 unit of **3**, respectively. This was further confirmed by COSY correlations (Fig. S9[†]) of H_3 -11/ H -8/ H_2 -9 and HMBC correlations from H_3 -11 to C-8, C-9, and the ketone carbonyl C-7 in the NMR spectra of **3**. Thus, the planar structure of **3** was assigned. ROESY correlations (Fig. S10[†]) of H_3 -13/ H -10a/ H_3 -14 suggesting their cofacial relationship, while ROESY correlations of H -10b/ H_3 -11 suggested that they were on the face opposite to H_3 -13. To determine the absolute configuration of **3**, its ECD spectrum was collected in MeOH and simulated at the B3LYP/6-311++G(2d,P) level after conformational optimization at the same level *via* Gaussian 05 software. The Boltzmann-weighted ECD curve for **3** agreed well with the experimental one (Fig. S11[†]), assigning its absolute configuration as (3*S*,4*R*,5*S*,8*S*)-.



Compound **4** had the molecular formula $C_{15}H_{26}O_2$, as established by its positive HRESIMS spectrum at m/z 261.1821 (calcd for $C_{15}H_{26}O_2Na$), indicating four degrees of unsaturation. The ^{13}C NMR and DEPT data of **4** showed the carbon resonances similar to those of **1**. Detailed comparison of the NMR data between **1** and **4** revealed that the main structural difference between them was the replacement of the C-6 hydroxyl methine in **1** by the C-6 conjugated ketone carbonyl in **4**, as supported by the HMBC correlations (Fig. 2) from both H_3-13 and $H-7$ to C-6 carbonyl. ROESY correlations (Fig. 3) of $H_3-14/H-10a$, $H_3-13/H-10a$ indicated the same direction of $H-3$ and $H-4$ and the different direction of H_3-13 . The calculated ECD spectrum for **4** match well with the experimental one (Fig. 5), thus assigning the absolute configuration of **4** as (3*S*,4*R*,5*R*)–.

Compound **5** was a colorless oil, had the same molecular formula $C_{15}H_{26}O_2$ as that of **1**, as established by its positive HRESIMS spectrum at m/z 261.1824 (calcd for $C_{15}H_{26}O_2Na$). The 1H and ^{13}C NMR data of **5** were quite similar to those of **1**. Detailed analysis of the NMR data of **5** revealed that the hydroxyl at C-6 in **1** was shifted to C-1 in **5**, as suggested by HMBC correlations from H_3-13 to the oxymethine carbon C-1 at δ_C 79.9 and the sp^3 methylene carbon C-6 at δ_C 40.8 and COSY correlations of $H-7/H_2-6$. The remaining substructure of **5** was determined to be the same as that of **1** by analysis of its 2D NMR data (Tables 1 and 2). In the ROESY spectrum, correlations (Fig. S10†) of $H_3-14/H-10a/H_3-13$ suggested the cofacial relationship of H_3-14 and H_3-13 . ROESY correlations of $H-6/H-4$ indicated that they were on the face opposite to H_3-13 . The Boltzmann-weighted calculated ECD curve of **5** agreed well with the experimental one (Fig. S11†), assigning its absolute configuration as (1*S*,3*R*,4*R*,5*S*)–.

Compound **6** was obtained as a colorless oil, had the molecular formula $C_{15}H_{24}O_3$ on the basis of HRESIMS, which indicated four degrees of unsaturation. The ^{13}C NMR spectral data of **6** were very similar to those of **2** except for the replacement of the hydroxyl methine C-7 and the methylene C-6 signals in **2** by signals at δ_C 204.3 and 87.3 corresponding to a conjugated ketone and a hydroxylated methine, respectively, in **6**. The above data, together with the HMBC correlations from H_3-13 to the hydroxylated methine C-6 and both H_3-11 and $H-6$ to the conjugated ketone C-7, indicated the –COH(6)–CO(7)– fragment. The remaining substructure of **6** was found to be identical to that of **2**, conjugated ketone C-7, indicated the –COH(6)–CO(7)– fragment. The remaining substructure of **6** was found to be identical to that of **2**, as confirmed by detailed interpretation of the 2D NMR data (Fig. S9†).

The relative configuration was established by analysis of the ROESY data (Fig. S10†). Correlations of $H-6/H-4$ revealed their cofacial relationship, while correlations of $H_3-14/H-10/H_3-13$ suggested that these protons were on the face opposite to $H-4$. The Boltzmann-weighted ECD curve for **6** agreed well with the experimental one (Fig. S11†), assigning its absolute configurations as 3*R*, 4*R*,5*R*, and 6*S*.

Compound **7** was obtained as a white powder, had the molecular formula $C_{15}H_{26}O_2$, as established by its positive HRESIMS spectrum at m/z 261.1829 (calcd for $C_{15}H_{26}O_2Na$), indicating three degrees of unsaturation. The 1H and ^{13}C NMR data of **7** were comparable to those of **2**, except for the

appearance of signals for a terminal alkenyl group ($\delta_{C/H}$ 113.1/4.88, 5.04) and a sp^3 methylene ($\delta_{C/H}$ 34.0/2.23, 2.29) and the disappearance of signals for the trisubstituted double bond C-8/C-9 and the C-11 methyl. COSY correlations (Fig. 2) of $H-4/H_2-10/H_2-9$ and $H_2-6/H-7$ and HMBC correlations from the olefinic protons H_2-11 to the hydroxylated methine C-7 and C-9 suggested that the double bond at C-8/C-9 in **2** shifted to C-8/C-11 in **7**. The remaining substructure of **7** was determined to be the same as that of **2** by analysis of the 2D NMR data (Fig. S9†). ROESY correlations (Fig. S10†) of $H_3-14/H-10/H_3-13/H-7$ led to the assignment of the relative configuration of **7** as shown in Fig. 3. The absolute configuration of **7** was assigned to be (3*S*,4*S*,5*S*,7*R*)– by comparison of its experimental ECD curve with the calculated one (Fig. S11†).

Biological activity

The cytotoxic activity of compounds **1–10** was tested against Huh-7 (human hepatoma carcinoma cell line), MCF-7 (human breast cancer cell line), MDA-MB-231 (human breast cancer cell line), A549 (human lung carcinoma cell line) and IDH1^{R132H} mutant by using the MTT method.¹⁶ Compound **10** showed cytotoxic to Huh-7, MCF-7, MDA-MB-231 cell lines and IDH1^{R132H} mutant, with IC_{50} values of 47.03 ± 2.48 , 38.33 ± 2.04 , 49.06 ± 1.81 , and $13.99 \mu M$, respectively. Compound **2** showed cytotoxic to MCF-7, with IC_{50} value of $43.38 \pm 7.22 \mu M$. Whereas the corresponding positive control DDP showed IC_{50} values of 7.55 ± 2.94 , 1.27 ± 0.18 , and $2.84 \pm 0.47 \mu M$, respectively. Compounds **1** and **3–9** were inactive against the tested cell lines at $50 \mu M$. Compound **4** and **9** showed potent inhibitory activities against the IDH1^{R132H} mutant, with IC_{50} value of $22.27 \pm 0.24 \mu M$ and $13.99 \pm 0.37 \mu M$.

Conclusions

In conclusion, seven undescribed carotane sesquiterpenoids named fusanoid A–G (**1–7**), along with one known analog (**8**) and two known sesterterpenes (**9** and **10**), and were isolated from the fermentation broth of the desert endophytic fungi *Fusarium* sp. HM166. Their chemical structures, including their absolute configurations, were determined by spectroscopic data, single-crystal X-ray diffraction analysis, and ECD calculations. In addition, this research provided a series of carotane sesquiterpenoids from the desert endophytic fungi. Our findings further suggested that the desert endophytic fungi is a rich source of bioactive secondary metabolites, and thus worthy of in-depth investigations.

Experimental

General experimental procedures

Optical rotation was measured at room temperature on a JASCO P-2000 polarimeter (JASCO, Easton, PA, USA) using a 1 cm cell. The IR spectra were obtained on with a Nicolet iS10. The NMR spectra were recorded on a Bruker AM-600 spectrometer with TMS as an internal standard. HREIMS data were acquired on a Thermo Scientific LTQ Orbitrap XL spectrometer. Semi-



preparative HPLC was performed on an Ultimate 3000 chromatographic system with a Thermo Hypersil Gold (10 × 250 mm, 3 mL min⁻¹). Thin-layer chromatography (TLC) and column chromatography (CC) were carried out on precoated silica gel (60–80 mesh, Qingdao Marine Chemical Inc., Qingdao, China) and silica gel (200–300 mesh, Qingdao Marine Chemical Inc., Qingdao, China), respectively.

Fungal material

The strain *Fusarium* sp. HM166 was isolated from Chenopodium quinoa, collected from Inner Mongolia Autonomous Region of west China, which was identified based on the rDNA ITS1–4 gene sequences (GenBank accession No. MK478900, ES1†) of the single colonies. A reference culture of *Fusarium* sp. HM166 is deposited in our laboratory and which maintained at –80 °C. The strain was grown on PDA plates at 28 °C for 5 days, then it was cut into small pieces and cultured in PDA liquid at 28 °C for 4 days to afford a seed culture. The fungus was cultured in 200 × 500 mL Erlenmeyer flasks each containing 200 mL of liquid medium (20 g mannitol, 20 g maltose, 10 g glucose, 10 g monosodium glutamate, 3 g yeast extract, 0.5 g corn meal, 0.5 g KH₂PO₄, 0.3 g MgSO₄).

Extraction and isolation

The fermented cultures were extracted with three-fold volumes of EtOAc, then the EtOAc solutions were combined and evaporated under reduced pressure to produce a dark brown solid crude extract. The extract was fractionated by a silica gel VLC column using different solvents of increasing polarity, from EtOAc–petroleum to yield thirteen fractions (Fr. 1–13). Fraction 2 was applied to octadecylsilane (ODS) silica gel with gradient elution of MeOH–H₂O (20 : 1, 30 : 1, 50 : 1, 60 : 1, 70 : 1, 1 : 0) to subfractions (Fr.2-1–Fr.2-6). Fr.2-5 was subjected to semipreparative HPLC (Thermo Hypersil Gold, 5 μm; 10 × 250 mm; 55% MeOH–H₂O; 3 mL min⁻¹) to give compound 3 (*t*_R 15 min; 10.0 mg). Fr.2-6 was subjected to semipreparative HPLC (Thermo Hypersil Gold, 5 μm; 10 × 250 mm; 40% MeCN–H₂O; 3 mL min⁻¹) to give compound 6 (*t*_R 32 min; 12.0 mg). Fraction 4 was applied to ODS silica gel with gradient elution of MeOH–H₂O (20 : 1, 30 : 1, 50 : 1, 60 : 1, 70 : 1, 80 : 1, 1 : 0) to subfractions (Fr.4-1–Fr.4-6). Fr.4-3 was subjected to semipreparative HPLC (Thermo Hypersil Gold, 5 μm; 10 × 250 mm; 56% MeCN–H₂O; 3 mL min⁻¹) to give compounds 5 (*t*_R 22.8 min; 9.3 mg) and 8 (*t*_R 32.6 min; 8.0 mg). Fr.4-4 was subjected to semipreparative HPLC (Thermo Hypersil Gold, 5 μm; 10 × 250 mm; 53% MeOH–H₂O; 3 mL min⁻¹) to give compounds 1 (*t*_R 34 min; 4.4 mg) and 7 (*t*_R 36.0 min; 6.8 mg). Fr.4-6 was subjected to semipreparative HPLC (Thermo Hypersil Gold, 5 μm; 10 × 250 mm; 78% MeOH–H₂O; 3 mL min⁻¹) to give compounds 9 (*t*_R 11.4 min; 18.9 mg) and 10 (*t*_R 14.1 min; 30.9 mg). Fraction 7 was applied to octadecylsilane (ODS) silica gel with gradient elution of MeOH–H₂O (20 : 1, 30 : 1, 50 : 1, 60 : 1, 70 : 1, 80 : 1, 1 : 0) to subfractions (Fr.7-1–Fr.7-6). Fr.7-1 was subjected to semipreparative HPLC (Thermo Hypersil Gold, 5 μm; 10 × 250 mm; 43% MeCN–H₂O; 3

mL min⁻¹) to give compounds 2 (*t*_R 12 min; 21 mg) and 4 (*t*_R 14 min; 3.2 mg).

Fusanoïd A (1). Colorless oil; [α]_D²⁵ + 40.1 (*c* 0.1, MeOH); UV (MeOH) λ_{max} (log ε): 201.0 (1.97); IR (KBr) ν_{max} (cm⁻¹): 3362, 2964, 2875, 1450, 1377, 1165, 1032, 1017. ¹H and ¹³C NMR data, Tables 1 and 2; HRESIMS *m/z* 261.1825 [M + Na]⁺ (calcd for C₁₅H₂₆O₂ Na, 261.1825).

Fusanoïd B (2). Colorless oil; [α]_D²⁵ – 47.3 (*c* 0.1, MeOH); UV (MeOH) λ_{max} (log ε): 202.5 (2.38); IR (KBr) ν_{max} (cm⁻¹): 3360, 2960, 2891, 1453, 1379, 1155, 1038, 1027. ¹H and ¹³C NMR data, Tables 1 and 2; HRESIMS *m/z* 261.1820 [M + Na]⁺ (calcd for C₁₅H₂₆O₂ Na, 261.1825).

Fusanoïd C (3). Colorless oil; [α]_D²⁵ + 90.8 (*c* 0.1, MeOH); UV (MeOH) λ_{max} (log ε): 240.0 (1.54); IR (KBr) ν_{max} (cm⁻¹): 3447, 2966, 2874, 1694, 1450, 1378, 1054. ¹H and ¹³C NMR data, Tables 1 and 2; HRESIMS *m/z* 261.1821 [M + Na]⁺ (calcd for C₁₅H₂₆O₂ Na, 261.1825).

Fusanoïd D (4). Yellow oil; [α]_D²⁵ – 30.0 (*c* 0.1, MeOH); UV (MeOH) λ_{max} (log ε): 240.0 (2.27); IR (KBr) ν_{max} (cm⁻¹): 3455, 2966, 1652, 1640, 1442, 1376, 1157. ¹H and ¹³C NMR data, Tables 1 and 2; HRESIMS *m/z* 259.1661 [M + Na]⁺ (calcd for C₁₅H₂₄O₂Na, 259.1669).

Fusanoïd E (5). Colorless oil; [α]_D²⁵ – 7.9 (*c* 0.1, MeOH); UV (MeOH) λ_{max} (log ε): 201.0 (2.32); IR (KBr) ν_{max} (cm⁻¹): 3420, 2966, 1678, 1594, 1456, 1373, 1140, 1032. ¹H and ¹³C NMR data, Tables 1 and 2; HRESIMS *m/z* 261.1824 [M + Na]⁺ (calcd for C₁₅H₂₆O₂Na, 261.1825).

Fusanoïd F (6). Yellow oil; [α]_D²⁵ + 60.9 (*c* 0.1, MeOH); UV (MeOH) λ_{max} (log ε): 243.5 (2.29); IR (KBr) ν_{max} (cm⁻¹): 3433, 2967, 1709, 1450, 1379, 1157, 1018. ¹H and ¹³C NMR data, Tables 1 and 2; HRESIMS *m/z* 275.1615 [M + Na]⁺ (calcd for C₁₅H₂₄O₃Na, 275.1615).

Fusanoïd G (7). Yellow oil; [α]_D²⁵ – 30.4 (*c* 0.1, MeOH); UV (MeOH) λ_{max} (log ε): 240.0 (2.27); IR (KBr) ν_{max} (cm⁻¹): 3346, 2967, 1700, 1460, 1382, 1154. ¹H and ¹³C NMR data, Tables 1 and 2; HRESIMS *m/z* 259.1661 [M + Na]⁺ (calcd for C₁₅H₂₄O₂Na, 259.1669).

X-ray crystallography

Data for compound 1. C₁₅H₂₆O₂, *M* = 238.18, *a* = 6.4271(19) Å, *b* = 8.2638(2) Å, *c* = 30.7804(11) Å, α = 90.00°, β = 90.00°, γ = 90.00°, *V* = 1634.81(9) Å³, *T* = 293 K, space group *P*2₁2₁2₁, *Z* = 4, μ(Cu Kα) = 0.580, 2784 reflections measured, 2921 independent reflections (*R*_{int} = 0.0427). The final *wR*(*F*²) values were 0.1133 (all data). CCDC: 2080924 (<https://www.ccdc.cam.ac.uk> (accessed on 29 April 2021)).

Cytotoxicity bioassays

All cells were purchased from the type culture collection of the Chinese Academy of Sciences (Shanghai, China). Cell proliferation rates were assessed using the MTT assay. Briefly, cells were seeded into 96-well plates at a density of 5000 cells per well. The experimental groups were treated with different concentrations of compounds ranging from 6.25 μM to 50 μM on the basis of glucose stimulation. After 48 h, MTT was added into each well at a concentration of 100 μg per well, incubated



Paper

for 4 h and then replaced with 100 μ L Tris-HCl. The number of viable cells was evaluated by measuring the absorbance at an OD of 570 nm using a Microplate Reader (Tecan, Mannedorf, Switzerland).¹⁶

Enzyme inhibition assays

Determination of the activity and inhibition of IDH1^{R132H} was based on the initial linear consumption of NADPH in the reaction. The enzyme activity assay was performed in a 96-well microplate by using the purified IDH1 mutant (0.4 μ M) in a buffer containing 1 M α -KG, 2 mM NADPH (\gg Km for NADPH) and 15 mM WST-8. For the inhibition assay, triplicate samples of the compounds were incubated with the protein for 5 min, before adding α -KG to initiate the reaction. The absorption peak was detected at 450 nm using a microplate reader, the experimental data were analyzed, and the IC₅₀ of each compound was calculated using GraphPad Prism.^{17,18}

Conflicts of interest

There are no conflicts to declare.

Acknowledgements

This research was funded by grants from National Key Research and Development Program of China (2017YFD0201401) and Changjiang Scholars and Innovative Research Team in University (IRT_15R16).

Notes and references

- 1 A. Cherif, G. Tsiamis, S. Compant and S. Borin, *BioMed Res. Int.*, 2015, 289457.
- 2 J. He, E. M. K. Wijeratne, B. P. Bashyal, J. Zhan, C. J. Seliga, M. X. Liu, E. E. Pierson, L. S. Pierson, H. D. VanEtten and A. A. L. Gunatilaka, *J. Nat. Prod.*, 2004, **67**, 1985–1991.
- 3 D. J. Newman and G. M. Cragg, *J. Nat. Prod.*, 2020, **83**, 770–803.
- 4 H. W. Zhang, Y. C. Song and R. X. Tan, *Nat. Prod. Rep.*, 2006, **23**, 753–771.
- 5 G. Ding, Y. C. Song, J. R. Chen, C. Xu, H. M. Ge, X. T. Wang and R. X. Tan, *J. Nat. Prod.*, 2006, **69**, 302–304.
- 6 M. González-Teuber, C. Vilo and L. Bascañán-Godoy, *Genomics Data*, 2017, **11**, 109–112.
- 7 M. Murgia, M. Fiamma, A. Barac, M. Deligios, V. Mazzarello, B. Paglietti, P. Cappuccinelli, A. Al-Qahtani, A. Squartini, S. Rubino and M. N. Al-Ahdal, *MicrobiologyOpen*, 2018, e00595.
- 8 I. Noy-Meir, *Annu. Rev. Ecol. Syst.*, 1973, **4**, 25–51.
- 9 J. D. A. Clarke, *Geomorphol.*, 2006, **73**, 101–114.
- 10 X. N. Wang, B. P. Bashyal, E. M. K. Wijeratne, J. M. U'Ren, M. X. Liu, M. K. Gunatilaka, A. E. Arnold and A. A. L. Gunatilaka, *J. Nat. Prod.*, 2011, **74**, 2052–2061.
- 11 Y. Y. Li, X. M. Tan, Y. D. Wang, J. Yang, Y. G. Zhang, B. D. Sun, T. Gong, L. P. Guo and G. Ding, *J. Nat. Prod.*, 2020, **83**, 1488–1494.
- 12 X. M. Tan, X. Y. Zhang, M. Yu, Y. T. Yu, Z. Guo, T. Gong, S. B. Niu, J. C. Qin, Z. M. Zou and G. Ding, *Phytochemistry*, 2020, **164**, 154–161.
- 13 B. P. Bashyal, B. P. Wellensiek, R. Ramakrishnan, S. H. Faeth, N. Ahmad and A. A. L. Gunatilaka, *Bioorg. Med. Chem.*, 2014, **22**, 6112–6116.
- 14 W. H. Ma, H. Huang, P. Zhou and D. F. Chen, *J. Nat. Prod.*, 2009, **72**, 676–678.
- 15 D. L. Guo, M. Zhao, S. J. Xiao, B. Xia, B. Wan, Y. C. Gu, L. S. Ding and Y. Zhou, *Phytochem. Lett.*, 2015, **14**, 260–264.
- 16 Z. Liu, Y. Tian, Q. Chen, G. Zhang, C. Li and D. Luo, *Anti-Cancer Agents Med. Chem.*, 2020, **20**, 417–428.
- 17 Y. X. Liu, W. W. Hua, Y. Li, X. R. Xian, Z. Zhao, C. Liu, J. J. Zou, J. Li, J. F. Xian and Y. B. Zhu, *Biochem. Pharmacol.*, 2015, **14**, 260–264.
- 18 Y. He, M. Z. Zheng, Q. Li, Z. Hu, H. C. Zhu, J. J. Liu, J. P. Wang, Y. B. Xue, H. Li and Y. H. Zhang, *Org. Chem. Front.*, 2013, 1–4.

